# Multigap superconductivity in the filled-skutterudite compound $LaRu_4As_{12}$ probed by muon spin rotation

A. Bhattacharyya [1,*] D. T. Adroja [2,3,†] M. M. Koza [4,‡] S. Tsutsui [5,6] T. Cichorek [7] and A. D. Hillier [2]

[1] *Department of Physics, Ramakrishna Mission Vivekananda Educational and Research Institute, Belur Math, Howrah 711202, West Bengal, India*

[2] *ISIS Facility, Rutherford Appleton Laboratory, Chilton, Didcot, Oxon, OX11 0QX, United Kingdom*

[3] *Highly Correlated Matter Research Group, Physics Department, University of Johannesburg, Auckland Park 2006, South Africa*

[4] *Institut Laue Langevin, 71 avenue des Martyrs, CS20 156, 38042 Grenoble Cedex 9, France*

[5] *Japan Synchrotron Radiation Research Institute, SPring-8, Sayo, Hyogo 679-5198, Japan*

[6] *Institute of Quantum Beam Science, Graduate School of Science and Engineering, Ibaraki University, Hitachi, Ibaraki 316-8511, Japan*

[7] *Institute of Low Temperature and Structure Research, Polish Academy of Sciences, 50-422 Wroclaw, Poland*

(Received 15 February 2022; revised 19 September 2022; accepted 22 September 2022; published 28 October 2022)

Muon spin rotation ($\mu$SR) and inelastic x-ray scattering were used to investigate the superconducting properties of the filled-skutterudite compound $LaRu_4As_{12}$. A two-gap isotropic ($s+s$)-wave model can explain the temperature dependence of the superfluid density. Zero-field $\mu$SR measurements confirm that the time-reversal symmetry does not break upon entering the superconducting state. The measurements of lattice dynamics at 2, 20, and 300 K revealed temperature dependences of the phonon modes that do not strictly follow a hardening of phonon frequencies upon cooling as expected within the quasiharmonic picture. The 20 K data rather mark a turning point for the majority of the phonon frequencies. Indeed, a hardening is observed approaching 20 K from above, while for a few branches a weak softening is visible upon further cooling to 2 K. The observed dispersion relations of phonon modes throughout the Brillouin zone matches with the density functional theory prediction quite closely. Our results point out that cubic $LaRu_4As_{12}$ is a good reference material for studying multiband superconductivity, including those with lower crystallographic symmetries such as iron arsenide–based superconductors.

DOI: 10.1103/PhysRevB.106.134516

## I. INTRODUCTION

Materials scientists and physicists have been intrigued by properties of the ternary transition metal pnictides ($Pn$) with the chemical formula $MT_4Pn_{12}$ ($M$ = alkali metal, alkaline-earth metal, lanthanide, or light actinide element; $T$ = Fe, Ru, or Os; $Pn$ = P, As, or Sb), which crystallize in the filled skutterudite structure with space group $Im\bar{3}$ (No. 204) [1]. Examples include excellent thermoelectric performance [2,3] and strongly correlated electron phenomena such as unconventional superconductivity [4–6], quadrupolar ordering [7–11], non-Fermi-liquid behavior [12], hybridization gap or Kondo phenomena [12–17], and unusual metal-insulator transitions [18]. From various factors that give rise to a plethora of unusal physical properties of $MT_4Pn_{12}$, the hybridization of localized $f$-electron states with conduction electron states is of prime importance. It was shown for $MRu_4As_{12}$ that the subtle interplay of the $Ru_4As_{12}$ sublattice with the $M$ cation results in multiband superconductivity, non-Fermi-liquid behavior, and conventional superconductivity, and low-lying ferromagnetic order for La [19], Ce [20], Pr [21], and Nd [22]. It is worth emphasizing that due to their cubic structure, $MT_4Pn_{12}$ compounds are unique in that they can be used to study multiband effects [23–25]. This opens an opportunity to compare and contrast multiband effects in the superconductivity of anisotropic materials, such as iron pnictides [26,27], heavy-fermion compounds [23,28–30], and topological insulators [31,32].

Most of the La-filled skutterudites exhibit BCS-type superconductivity with the superconducting critical temperature $T_c$ ranging from 0.4 to 10.4 K [24,25]. Among all completely filled compounds $LaT_4Pn_{12}$, $LaRu_4As_{12}$ shows the highest transition temperature accompanied by the highest upper critical field $H_{c2}(0)$ [33]. These parameters are substantially enhanced compared to the sister compounds $LaOs_4As_{12}$ [34] and $PrRu_4As_{12}$ [35], with $T_c = 3.2$ and 2.3 K, respectively. This enhancement is even more intriguing if one takes into account that $LaRu_4As_{12}$ does not show any distinct differences in both the conduction electron density of states at the Fermi level and the vibrational properties [36,37]. Another remarkable feature of $LaRu_4As_{12}$ is that it has several arguments for multiband superconductivity [1–5,33,36]. Specifically, the temperature dependence of the lower critical field $H_{c1}$ displays a sharp anomaly deep in the superconducting state, indicative of a rarely observed case of almost decoupled bands [33]. Furthermore, a very recent observation of suppression of anharmonic phonons by artificial nonmagnetic defects is in

*amitava.bhattacharyya@rkmvu.ac.in
†devashibhai.adroja@stfc.ac.uk
‡koza@ill.fr

 

line with multiband superconductivity in the filled skutterudite $LaRu_4As_{12}$ [38]. Considering all of these factors, we are compelled to investigate this compound further.

In this work, we investigate $LaRu_4As_{12}$ utilizing muon spin rotation and relaxation ($\mu$SR), as well as inelastic x-ray scattering (IXS) measurements. $\mu$SR is a microscopic and very sensitive technique and provides direct information about the gap symmetry from the temperature dependence of superfluid density measured using transverse field (TF) $\mu$SR. Further, zero-field (ZF) $\mu$SR is very sensitive and can detect a very small local magnetic field inside the (type II) superconducting state and hence can provide direct information on the broken time-reversal symmetry. Inelastic x-ray scattering provides direct information about phonon dispersion, and hence, it is very important to investigate the change in the phonon dispersion above and below the superconducting transition in $LaRu_4As_{12}$. These measurements are important for understanding the mechanism of the superconductivity in $LaRu_4As_{12}$. Using TF-$\mu$SR measurements, we show clear evidence of multiband superconductivity in $LaRu_4As_{12}$. As a result, in addition to Fe-based and cuprate superconductors, $LaRu_4As_{12}$ could be a unique multiband superconductor [19]. The preservation of time-reversal symmetry is revealed by studying ZF-$\mu$SR. The observed phonon dispersion, using IXS, shows good agreement with the density functional theory (DFT)-calculated phonon dispersion.

## II. EXPERIMENTAL DETAILS

Single crystals of $LaRu_4As_{12}$ were grown by mineralization in a molten Cd:As flux using a procedure previously reported [39]. The low-temperature electrical resistivity of a $LaRu_4As_{12}$ single crystal was investigated by a conventional four-point ac technique using a $^4$He cryostat (physical property measurement system). Magnetic measurements for a collection of $LaRu_4As_{12}$ single crystals were performed down to 1.8 K at $\mu_0 H = 3$ mT utilizing a superconducting quantum interference device magnetometer (magnetic property measuring system). The MUSR spectrometer at the ISIS Pulsed Neutron and Muon Source, Rutherford Appleton Laboratory, United Kingdom, was used to measure the muon spin rotation and relaxation of $LaRu_4As_{12}$.

The powder sample (1 g) of $LaRu_4As_{12}$ obtained from very small single crystals was mounted on a silver holder using diluted GE varnish (99.999%). This was placed on the dilution refrigerator's cold finger. Zero-field and transverse field measurements were taken at temperatures ranging from 0.31 to 13.0 K. For ZF measurements, an active correction coil was employed to cancel any stray magnetic fields in the sample space to a level of $10^{-4}$ mT. The ZF-$\mu$SR measurement assists us in identifying the spontaneous internal field associated with time-reversal symmetry breaking [40]. The TF-$\mu$SR measurements were carried out in the presence of a 40 mT external magnetic field, which is higher than the lower critical field ($\mu_0 H_{c1} = 1.3$ mT) and significantly lower than the upper critical field ($\mu_0 H_{c2} = 10.3$ T) of $LaRu_4As_{12}$ [48]. To avoid any flux trapping effects, we applied the transverse field at temperature much higher than $T_c$ and subsequently cooled the sample down to base temperature. The WIMDA software was used to evaluate the experimental data [41].

High-resolution IXS experiments were carried out at the beamline BL35XU of the SPring-8 synchrotron radiation facility in Harima, Japan [42]. Si(11 11 11) backscattering optics with 21.747 keV photon energy was chosen for the present work, resulting in an energy resolution of 1.5 meV. The $Q$ resolution was set to (0.06 0.06 0.06) in reciprocal lattice units along the [1 0 0] and [1 1 0] directions. Constant $Q$ scans were carried out in an extended range of reciprocal space at temperatures of 2, 20, and 300 K. A few supplementary scans were performed at 6 and 14 K, i.e., below and above $T_c$. The sample temperature was controlled by a helium closed-cycle refrigerator. The quality of the single-crystal sample was checked by measuring the rocking curve widths on a series of Bragg reflections along with high-symmetry directions, say, [100], [110], and [001]. These widths are less than 0.1° and close to the resolution limit of the BL35XU spectrometer, ∼0.02°. Phonon properties of $LaRu_4As_{12}$ were modeled by DFT-based lattice dynamics calculations. The first-principles calculations were performed with the Vienna Ab initio Simulation Package (VASP) utilizing projector augmented wave potentials and the generalized gradient approximation of Perdew, Burke, and Ernzerhof (GGA-PBE) for the exchange-correlation terms [43–45]. The electronic minimization and the subsequent calculation of Hellmann-Feynman (HF) forces, were carried out with a $2 \times 2 \times 2$ supercell and a Monkhorst-Pack $k$ mesh of $4 \times 4 \times 4$ [46]. The first-order Methfessel-Paxton method with $\sigma = 0.1$ for the band occupancies was applied, and forces were relaxed to $10^{-7}$. The relaxed structure resulted in a lattice parameter of $a = 8.6074$ Å and fractional coordinates of $y = 0.3497$ and $z = 0.1507$ for the As position. The dynamical matrix and thus the phonon eigenvectors and eigenstates were derived from the HF forces using the direct method implemented in the software package PHONON [47]. The HF forces were computed for symmetry nonequivalent displacements of 0.03 Å in the high-symmetry directions of the atoms. For the estimation of phonon intensities, the eigenvectors were scaled by the atom-specific squared electron number $Z^2$ and an averaged electronic form factor. Within the dynamic range given by the experimental setup, the highest phonon intensities were derived for $Q$ numbers around the (600) Bragg reflection and the high-symmetry directions [600] → [611] and [600] → [700] → [6.5.5.5].

## III. RESULTS AND DISCUSSION

### A. Structure and physical properties

$LaRu_4As_{12}$ has a bcc structure with space group $Im\bar{3}$ (No. 204) which crystallizes in the $CoAs_3$-type skutterudite structure packed with La atoms. Figure 1(a) shows the structure, with green atoms for La, yellow for Ru, and red for As. The electropositive element La, which lacks fourfold rotational symmetry, is at the center of the large icosahedron cage formed by As atoms. Ru, a transition metal ion, creates a primitive cubic sublattice between the cages. The atomic positions are (0, 0, 0) for one La atom in the crystallographic position 2$a$, (1/4, 1/4, 1/4) for four Ru atoms in 8$c$, and (0, $y$, $z$) for 12 As atoms in 24$g$, with $y = 0.3499$ and $z = 0.1502$. Figure 1(b) displays the temperature variation of the resistivity in the zero applied magnetic field at the low-temperature limit.

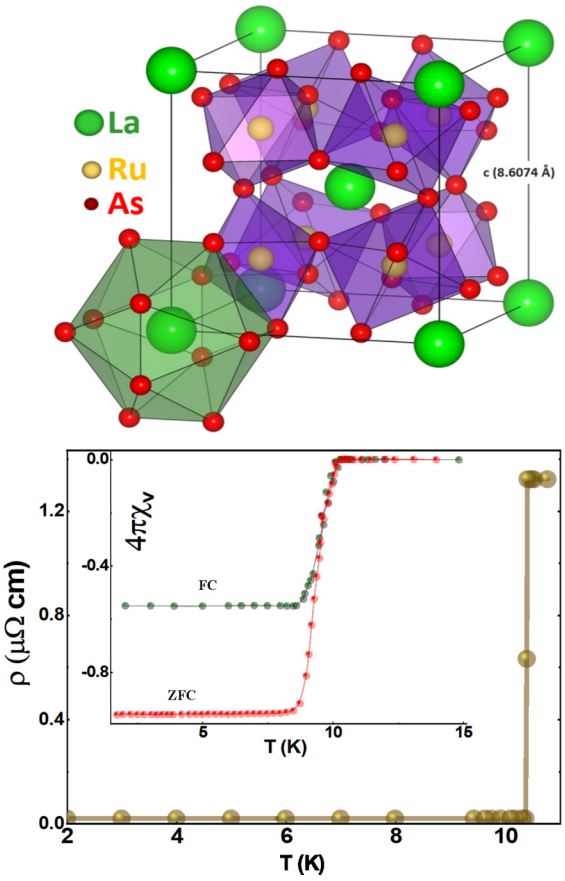


FIG. 1. Top: The bcc structure of the filled skutterudite $LaRu_4As_{12}$ with space group $Im\bar{3}$. Bottom: The low-temperature electrical resistivity of $LaRu_4As_{12}$ showing a sharp superconducting transition at 10.4 K. Inset: Zero-field-cooled (ZFC) and field-cooled (FC) magnetization in the presence of 3 mT applied field as a function of temperature for a collection of $LaRu_4As_{12}$ single crystals.

The drop of the electrical resistivity reveals superconductivity at $T_c = 10.4$ K. The low residual resistivity data revealed the good quality of the sample. The superconducting volume fraction in the $LaRu_4As_{12}$ sample was calculated using magnetization measurements. The inset of Fig. 1(b) shows the magnetization data for both zero-field-cooled (ZFC) and field-cooled (FC) measurements. In the ZFC measurement, full diamagnetic shielding is observed below $T_c = 10.4$ K.

### B. Superconducting gap structure: TF-$\mu$SR

To further understand the multiband nature of superconductivity as suggested by earlier experimental [48] and theoretical [36] studies, we performed TF-$\mu$SR measurements in $LaRu_4As_{12}$. The TF-$\mu$SR muon spin precession signals collected at $T = 12.5$ and 0.31 K in $\mu_0 H = 40$ mT are shown in Figs. 2(a) and 2(b). Due to the flux line lattice state, which causes spatial inhomogeneity of the magnetic field distribution below $T_c$, the data in Figs. 2(a) and 2(b) indicate a distinct contrast in the relaxation rate above and below $T_c$. The maximum entropy plots in Figs. 2(c) and 2(d) show one peak at 12.5 K at the applied field. An extra peak at 0.31 K is observed on the lower side of the applied field in addition to the peak at

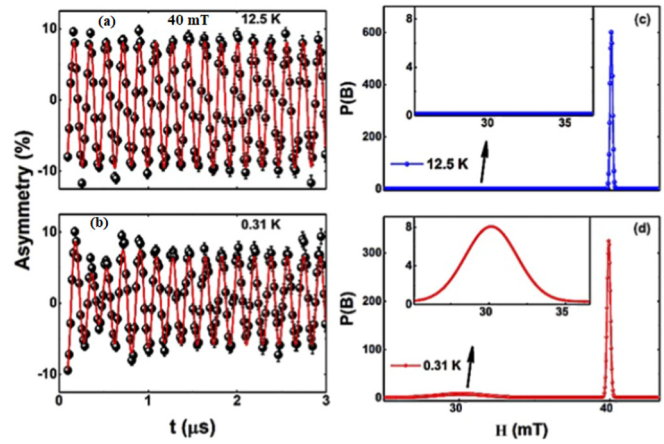


FIG. 2. (a) and (b) The asymmetry spectra of the TF-$\mu$SR data in the short-time region, obtained in a 40 mT applied magnetic field at $T = 12.5$ K (i.e., above $T_c$) and $T = 0.31$ K (i.e., below $T_c$), respectively. (c) and (d) The maximum entropy plots at $T = 12.5$ K and $T = 0.31$ K, respectively. A zoomed-in section of the low-field region is shown in the inset.

40 mT, confirming type-II superconductivity in this sample. Using straight Fourier transformation to extract frequency spectra from transverse $\mu$SR data is not practicable since at long times the data are noisy since the count rate is low due to the shortness of the muon lifetime. On the other hand, the maximum entropy method overcomes this problem and allows simultaneous analysis of spectra from multiple detectors with different phases to yield a single frequency spectrum [49]. The inset in Fig. 2(d) shows a zoomed-in section of the low-field region of the maximum entropy plot, which reveals a broad peak near 30 mT associated with the vortex lattice formation.

Due to the single peak of the internal field in the superconducting state, we fitted the data using a Gaussian function with one component. To illustrate the characteristics of the vortex state, we fitted the data using the expression [50–53]

$$A_{\mathrm{TF}}(t) = A_0 \cos(\gamma_\mu H_0 t + \Phi) \exp\left(-\frac{\sigma^2 t^2}{2}\right) + A_{\mathrm{bg}} \cos(\gamma_\mu H_{bg} t + \Phi), \quad (1)$$

where the first component is the sample contribution and the second is the background contribution. The initial asymmetries of the sample and silver holder contributions are described by $A_0$ and $A_{bg}$, respectively, where $A_{bg}$ does not undergo any depolarization; the internal fields of the sample and sample holder are described by $H_0$ and $H_{bg}$, respectively. The muon gyromagnetic ratio is $\gamma_\mu/2\pi = 135.53$ MHz/T; $\sigma$ is the Gaussian muon spin relaxation rate, and $\Phi$ is the initial phase of the signal at the detectors. The values of $A_0 = 0.66(1)$ and $A_{bg} = 0.34(1)$ were estimated by fitting 0.31 K data, and were kept fixed during the analysis of other temperature data. The superconducting depolarization rate can be determined by subtracting the nuclear contribution: $\sigma_{\mathrm{sc}} = \sqrt{\sigma^2 - \sigma_{\mathrm{n}}^2}$, where $\sigma_{\mathrm{n}} = 0.047\,\mu\mathrm{s}^{-1}$ is the normal state contribution, which is temperature independent, as is evident in spectra above $T_c$. Since $\sigma_{\mathrm{sc}}$ is connected to the magnetic penetration depth $\lambda$ by $\sigma_{\mathrm{sc}} \approx 1/\lambda^2$ for a triangular lattice [40,54], the temperature variation of $\sigma_{\mathrm{sc}}(T)$ can be used to measure the nature of the

superconducting gap. Then, using the functional form given below, single- and two-gap $s$-wave models are fitted to the data:

$$\frac{\sigma_{sc}(T)}{\sigma_{sc}(0)} = \frac{\lambda^{-2}(T)}{\lambda^{-2}(0)} = w\frac{\lambda^{-2}(T,\Delta_{0,1})}{\lambda^{-2}(0,\Delta_{0,1})} + (1-w)\frac{\lambda^{-2}(T,\Delta_{0,2})}{\lambda^{-2}(0,\Delta_{0,2})}, \quad (2)$$

where $\lambda(0)$ is the value of the penetration depth at $T = 0$ K, $\Delta_{0,i}$ is the value of the $i$th ($i = 1$ or 2) superconducting gap at $T = 0$ K, and $w$ is the weighting factor of the first gap. Each term in Eq. (2) is evaluated using the standard expression within the local London approximation ($\lambda \gg \xi$) [55] as

$$\frac{\sigma_{sc}(T)}{\sigma_{sc}(0)} = \frac{\lambda^{-2}(T,\Delta_{0,i})}{\lambda^{-2}(0,\Delta_{0,i})} = 1 + \frac{1}{\pi}\int_0^{2\pi}\int_{\Delta(T,\phi)}^{\infty}\left(\frac{\partial f}{\partial E}\right)\frac{E\,dE\,d\phi}{\sqrt{E^2-\Delta_i^2(T,\phi)}}, \quad (3)$$

where $f = [1+\exp(E/k_BT)]^{-1}$ is the Fermi function and the temperature and angle-dependent gap function are expected to follow the relationship $\Delta_i(T,\phi) = \Delta_{0,i}\delta(T/T_C)g(\phi)$. Here $\Delta_{0,i}$ denotes the maximum gap value at zero temperature, and $g(\phi)$ is the angular dependence of the gap; $g(\phi) = 1$ for an isotropic $s$-wave model and for $(s+s)$-wave gaps. Here $\phi$ is the azimuthal angle. The temperature dependence of the superconducting gap symmetry is expected to follow, $\delta(T/T_C) = \tanh\{1.82[1.018(T_C/T-1)]^{0.51}\}$ [56,57]. At any coupling strength, this gap function is accurate enough to explain the temperature dependency.

The symmetry of the superconducting gap was determined by fitting the data of $\lambda^{-2}(T)$ or $\sigma_{sc}(T)$ using (a) a single-gap $s$-wave model and (b) a multigap $(s+s)$-wave gap model, as presented in Fig. 3(a). Because it produces a high $\chi^2$ goodness of fit value [here $\chi^2 = \sum(\sigma_{obs}-\sigma_{cal})^2/\sigma^2_{error}(M-N)$, the total number of data points is $M$, and the number of free parameters is $N$], the typical BCS single gap cannot characterize the $\lambda^{-2}(T)$ data. A recent study of $LaRu_4As_{12}$ by Juraszek *et al.* [48] confirmed that the lower critical field behavior is well suited to multiband isotropic $s$-wave superconductivity. The multiband character of $LaRu_4As_{12}$ is further strengthened by the two-gap model employing the isotropic $s+s$ wave with $\chi^2 = 1.3$, compared to $\chi^2 = 3.1$ for a single-gap $s$-wave fit. The estimated larger gap is $2\Delta_1(0)/k_BT_C = 3.73 \pm 0.2$ in the $(s+s)$-wave model, which is close to the value of 3.53 derived from BCS theory, and the estimated smaller gap is $2\Delta_2(0)/k_BT_C = 0.144 \pm 0.01$ in the $(s+s)$-wave model. The smaller value of the second gap is observed in many Fe-based superconductors; for example, for $RbCa_2Fe_4As_4F_2$, $2\Delta_1/k_BT_C = 6.48$ and, $2\Delta_2/k_BT_C = 0.7$ ($T_C = 29.2$ K; see Table I of Ref. [51]). The different size of the gaps arises from the Fermi surface topology. Multigap features are common in iron-based superconductors, e.g., $Ba_{1-x}K_xFe_2As_2$ [58,59], cuprate superconductors [60], and also in $Bi_4O_4S_3$ [61]. We calculated the values of the London penetration depth $\lambda_L(0) = 240(4)$ nm for the $(s+s)$-wave fit, carrier density $n_s = 8.6(3)\times10^{27}$ carriers m$^{-3}$, and effective mass of the quasiparticle $m^* = 1.749(2)m_e$ for $LaRu_4As_{12}$ using the

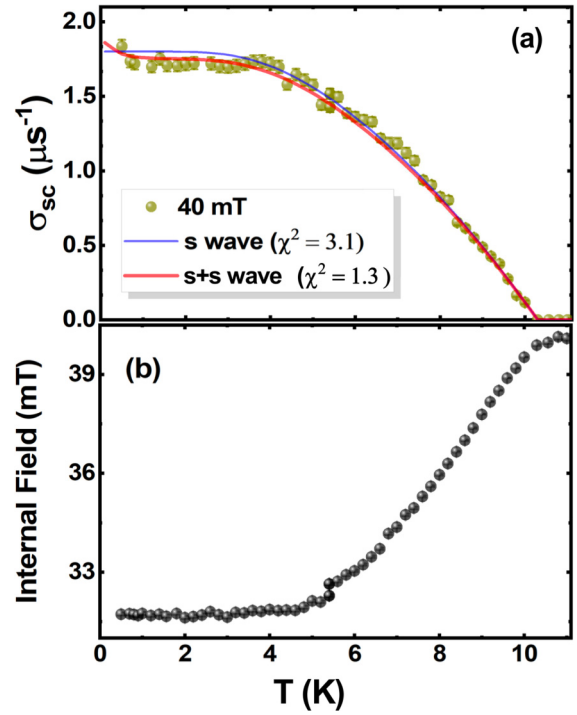


FIG. 3. (a) The temperature dependence of $\sigma_{sc}(T)$ data with fits to various gap models. The red line shows the fit to the two-gap $(s+s)$-wave model, while the blue line shows the fit to the single-gap isotropic $s$-wave model. (b) Temperature variations in the internal field confirm the appearance of the Meissner state.

method described in Refs. [62–64]. As shown in Fig. 3(b), the internal field of the flux line lattice is temperature dependent and decreases with decreasing temperature, as in other superconductors, indicating a diamagnetic shift. Because of the formation of a flux line lattice in the superconducting state, the total internal field inside the sample is reduced.

### C. Time-reversal symmetry: ZF-$\mu$SR

Here we present our ZF-$\mu$SR results for detecting the spontaneous internal field associated with time-reversal symmetry breaking in the superconducting state. As shown in Fig. 4, we measured the time evolution of ZF asymmetry spectra in both the normal and superconducting states. The ZF-$\mu$SR spectra were fitted using a combination of Lorentzian and Gaussian Kubo-Toyabe relaxation functions [52,65]:

$$A_{ZF}(t) = A_2G_{KT}(t)e^{-\lambda_{ZF}t} + A_{bg}, \quad (4)$$

where

$$G_{KT}(t) = \left[\frac{1}{3} + \frac{2}{3}(1-\sigma_{KT}^2t^2)\exp\left(-\frac{\sigma_{KT}^2t^2}{2}\right)\right] \quad (5)$$

TABLE I. Fitted parameters obtained from the fit to the $\sigma_{sc}(T)$ data of $LaRu_4As_{12}$ using different gap models.

| Model | $\Delta_i(0)$ (meV) | $2\Delta_i(0)/k_BT_C$ | $w$ | $\chi^2$ |
|---|---|---|---|---|
| $s$ wave | 1.59 | 3.57 | 1 | 3.1 |
| $s+s$ wave | 1.656, 0.064 | 3.73, 0.144 | 0.87 | 1.3 |

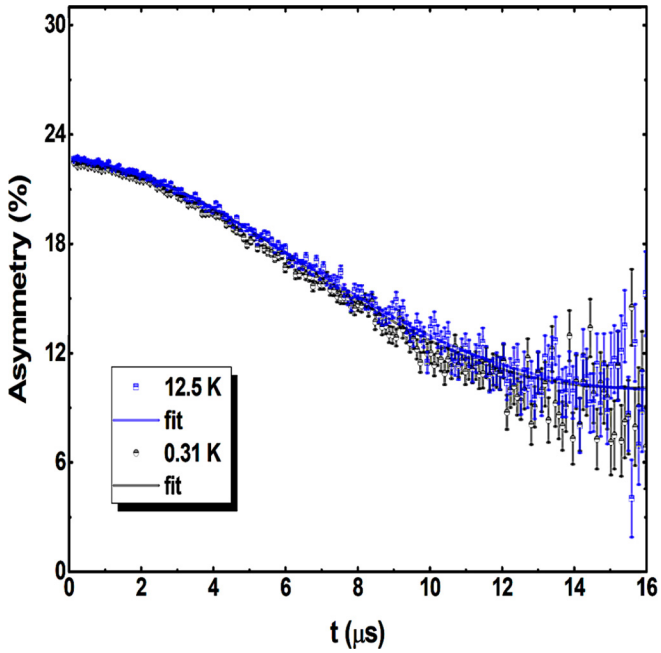


FIG. 4. The ZF-$\mu$SR spectra for $LaRu_4As_{12}$ at 0.31 K (black) and 12.5 K (blue). As stated in the text, the solid line fits the data.

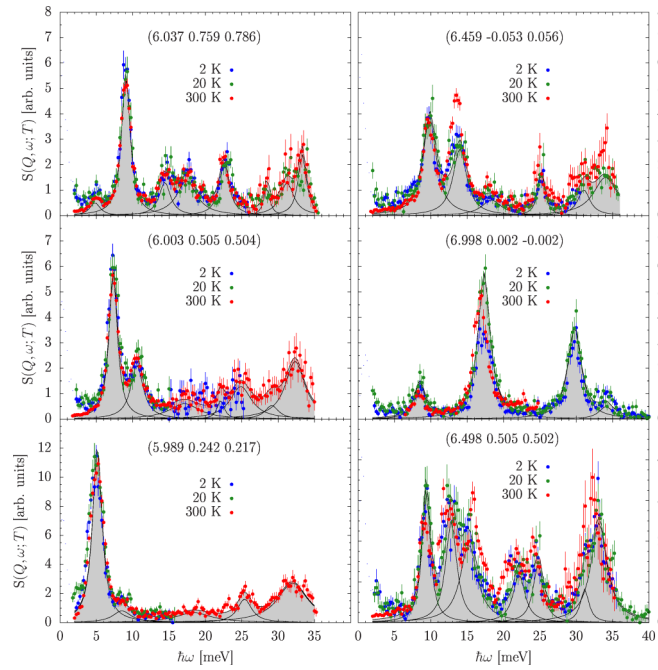


FIG. 5. Selected spectra of $LaRu_4As_{12}$ recorded along high-symmetry directions at the three different $T$ indicated in the plots. Lines with data correspond to standard Lorentzians fitted to the data (300 K in the left panel and 20 K in the right panel). Filled areas highlight the total fit functions.

is the Gaussian Kubo-Toyabe function and the sample and silver holder asymmetry contributions are represented by $A_2$ and $A_{bg}$, respectively. As shown in Fig. 4, both asymmetry spectra fall on top of each other, indicating that there is no change in relaxation rate in the superconducting state compared to the normal state. This denotes the lack of a spontaneous internal field. As a result, time-reversal symmetry is preserved in the superconducting state. Furthermore, the fits to the ZF data yield $\sigma_{KT} = 0.11(1)\,\mu s^{-1}$ and $\lambda_\mu = 0.010(2)\,\mu s^{-1}$ at 0.31 K and $\sigma_{KT} = 0.105(3)\,\mu s^{-1}$ and $\lambda_\mu = 0.011(2)\,\mu s^{-1}$ at 12.5 K.

### D. Inelastic x-ray scattering

As outlined above, we have investigated the lattice dynamics of the multiband superconductor $LaRu_4As_{12}$ ($T_c = 10.3$ K) by IXS at 300, 20, and 2 K. All spectra recorded at those $T$ are reported in Figs. 1–7 of the Supplemental Material [66]. For the highest intensities, the measurements were focused near the (6, 0, 0) Bragg position by performing longitudinal and transverse scans. Figure 5 shows some selected spectra recorded along high-symmetry directions at the sampled temperatures of 300, 20, and 2 K. It can be seen that the overall behavior of the compound is rather harmonic. No strong phonon renormalization can be identified over the entire explored temperature range. This applies not only to the high-symmetry directions shown in Fig. 5 but also to any other direction examined.

All spectra were fitted after the temperature correction with the Bose occupation number. Experimentally determined resolution functions were convoluted with the fitted model. The model was formed from a set of standard Lorentzian functions whose number was adjusted to the number of peaks identified. To compare data recorded at the three different temperatures the final fits were carried out only to the Stokes line data. However, we confirmed that both side fits of the spectra at 300 K resulted in very similar parameters. Differences might be attributed to the strong elastic line in the prior data treatment, which has been suppressed in the final fits.

Figure 6 reports all derived phonon energies along high-symmetry directions compared with our DFT computed dispersion relation and the total and partial phonon densities of states $Z(\omega)$. Note that for the best match, the energy scale of the DFT data has been scaled up by 7%. This underestimation of eigenfrequencies and overestimation of structural dimensions is a well-known feature of the GGA-PBE and was reported before [37,67]. The size of the energy symbols reflects the measured peak intensities on a logarithmic scale, and the peak widths are indicated by error bars. Vertical arrows indicate the **Q** points at which the spectra shown in Fig. 5 have been recorded.

Improving the statistical significance of the spectra was necessary to derive a conclusion on the temperature dependence of the phonon modes. $S(\mathbf{Q}, \omega)$ spectra from different analyzers recorded at a fixed setup were corrected for zero shift of the elastic line and merged to a generalized $S(\omega)$ signal. An example of the resulting data is presented in Fig. 7. All spectra have been fitted with standard Lorentzians accounting for the resolution function by convolution as well as the Bose thermal occupation. Figure 8 reports the frequencies derived from those fits. Different temperatures monitored in a single setup are indicated by different colors. Open symbols indicate less reliable frequencies which are strongly biased by the presence of the elastic line, on the one hand, and a strong localized mode, on the other.

Frequencies for which a switchover from hardening (going from 300 to 20 K) to softening upon cooling below $T_C$ (going

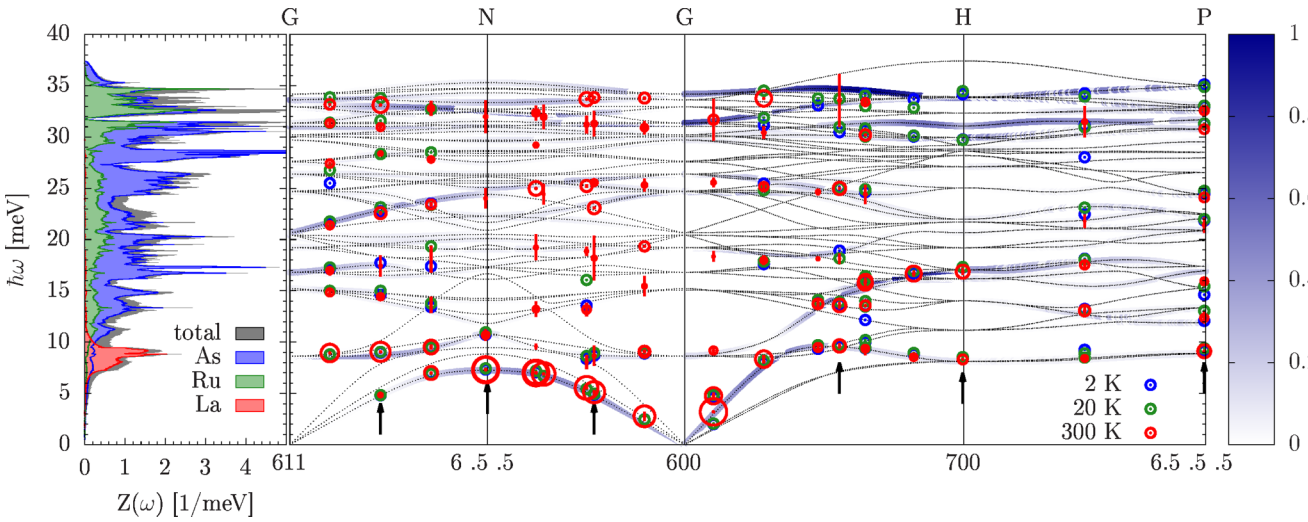


FIG. 6. Left: Total and partial phonon densities of states of $LaRu_4As_{12}$ computed with DFT and normalized to 51 phonon modes in the total signal. Right: Phonon energies derived from the Lorentzian fits. Symbol sizes correspond to the logarithm of the peak intensities, and error bars indicate the FWHM of the peaks. Dotted lines with the data report the DFT-computed phonon dispersion relation. The blue shaded signal indicates the DFT-computed phonon intensities. The energy scale of both $Z(\omega)$ and the phonon dispersion has been scaled up by 7% for a better match with the experimental data.

from 20 to 2 K) is observed are highlighted by the dashed black boxes in Fig. 8. Some other frequencies showing a softening already below 300 K are framed by dotted red boxes. The mode hardening between 300 and 20 K can be associated with the lattice contraction and is understandable within the theory of quasiharmonic crystals. Clearly, the mode softening below $T_C$ does not follow this classical quasiharmonic concept. It rather points at a weak electron-phonon coupling effect when entering the superconducting state below 10.5 K. This observation is supported by the theoretically calculated $T_c = 11.56$ K based on the electron-phonon coupling compared to the measured $T_c = 10.45$ K for $LaRu_4As_{12}$ [67].

Note that the significance of the conclusion upon the detectability of the electron-phonon coupling in the present IXS

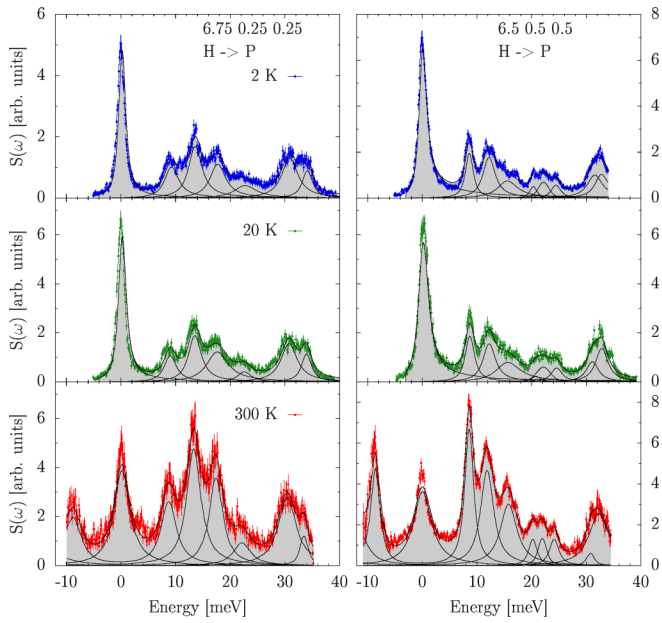


FIG. 7. Generalized spectra $S(\omega)$ at $T = 2$, 20, and 300 K from top to bottom. Left and right: Data are from scans for the high-symmetry midpoint and the end-point scan in the direction $H \rightarrow P$, respectively. Lines with data correspond to standard Lorentzians fitted to the data. The gray shaded area highlights the fitted total signal.

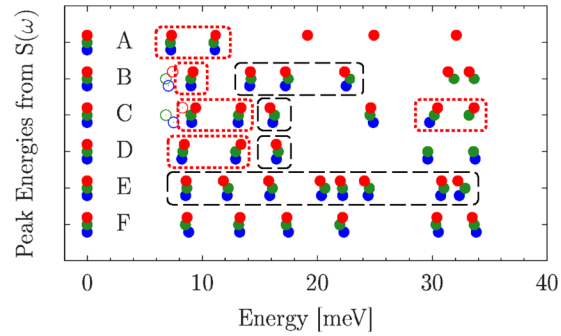


FIG. 8. Temperature dependence of peak energies derived through Lorentzian fits to the generalized $S(\omega)$ spectra. Different $T$ are indicated by the different colors: blue, 2 K; green, 20 K; red, 300 K. Letter labels indicate the different setups applied: A, $\Gamma \rightarrow N$, 600 $\rightarrow$ 6.5.5; B, $\Gamma \rightarrow N$, 6.5.5 $\rightarrow$ 611; C, $\Gamma \rightarrow H$, 600 $\rightarrow$ 6.500; D, $\Gamma \rightarrow H$, 6.500 $\rightarrow$ 700; E, $H \rightarrow P$, 6.5.5.5; F, $H \rightarrow P$, 6.75.25.25. Results for E and F are highlighted in Fig. 7, and those for all other orientations are in Fig. 8 of the Supplemental Material [66]. Boxes framed by dashed black lines highlight frequencies at which a turnover from mode hardening to softening upon cooling is particularly obvious. Boxes framed by dotted red lines indicate frequencies at which a softening is observed below 300 K not in line with a standard quasiharmonic response. See text for details. The symbol size approximates a diameter of 1 meV. The corresponding reliability parameters of the fits are reported in Table I of the Supplemental Material [66]. They are of the order of 0.1 meV.

data is qualified by the statistics of the results. Further experiments are required to understand whether specific vibrational eigenmodes are particularly involved in the electron-phonon interaction. The participation of specific eigenmodes would result in a characteristic directional dependence of the phonon response and should be studied in future experiments.

## IV. CONCLUSION

In conclusion, we have determined the superconducting state of $LaRu_4As_{12}$ using TF-$\mu$SR, and its lattice dynamics has been studied by inelastic x-ray scattering. The temperature dependence of the magnetic penetration depth was found to be consistent with a two-gap $(s+s)$-wave model of multiband superconductivity. The larger gap to $T_c$ ratio calculated within the $(s+s)$-wave scenario, $2\Delta_1(0)/k_BT_c = 3.73 \pm 0.2$, is very close to the value of 3.53 for an ordinary BCS superconductor. The ZF-$\mu$SR spectra at 0.31 and 12.5 K resemble each other very closely, indicating that the time-reversal symmetry is preserved in the superconducting state of $LaRu_4As_{12}$. Furthermore, IXS analyses of the Brillouin region reveal phonon modes between 300 and 20 K that show a weak temperature dependence which can be understood as an effect of the crystal's volume changes. In comparison to those at 20 K, many of the 2 K modes show a weak softening of the phonon frequencies, indicating that the electron-phonon interactions driving the superconductivity of $LaRu_4As_{12}$ exert a visible effect on the vibrational eigenstates. This observation is also in agreement with the theoretically calculated $T_c = 11.56$ K based on the electron-phonon coupling compared to the measured $T_c = 10.45$ K [67]. From a broader perspective our findings should be relevant for a wider class of multiband superconductors, including those with lower crystallographic symmetries such as iron arsenide superconductors.

## ACKNOWLEDGMENTS

We are grateful to Prof. T. Das and P. Adhikari for their insightful discussion on superconducting gap structure. We are grateful to Prof. Z. Henkie for providing single crystals of $LaRu_4As_{12}$. A.B. thanks the Science & Engineering Research Board for the CRG Research Grant (Grant No. CRG/2020/000698). The IXS experiment was performed under the approval of JASRI (Proposal No. 2018B1493). D.T.A. would like to acknowledge the funding from the Royal Society of London for the Newton Advanced Fellowship between the United Kingdom and China and for the International Exchange between the United Kingdom and Japan and EPSRC-UK (Grant Reference No. EP/W00562X/1). M.M.K. acknowledges the financial support by the Institut Laue Langevin (ILL) and technical support by the C-Lab of the ILL. We thank the ISIS facility for MuSR beam time RB1610522 [68].

[1] R. E. Baumbach and M. B. Maple, Filled skutterudites: Magnetic and electrical transport properties, in *Encyclopedia of Materials: Science and Technology*, edited by K. H. J. Buschow, M. C. Flemings, B. Ilschner, E. J. Kramer, S. Mahajan, and P. Veyssière's (Elsevier, Oxford, 2010), pp. 1–6.

[2] B. C. Sales, D. Mandrus, and R. K. Williams, Science **272**, 1325 (1996).

[3] V. Keppens, D. Mandrus, B. C. Sales, B. C. Chakoumakos, P. Dai, R. Coldea, M. B. Maple, D. A. Gajewski, E. J. Freeman, and S. Bennington, Nature (London) **395**, 876 (1998).

[4] E. D. Bauer, N. A. Frederick, P.-C. Ho, V. S. Zapf, and M. B. Maple, Phys. Rev. B **65**, 100506(R) (2002).

[5] H. Kotegawa, M. Yogi, Y. Imamura, Y. Kawasaki, G.-q. Zheng, Y. Kitaoka, S. Ohsaki, H. Sugawara, Y. Aoki, and H. Sato, Phys. Rev. Lett. **90**, 027001 (2003).

[6] D. T. Adroja, A. D. Hillier, J.-G. Park, E. A. Goremychkin, K. A. McEwen, N. Takeda, R. Osborn, B. D. Rainford, and R. M. Ibberson, Phys. Rev. B **72**, 184503 (2005).

[7] K. Hachitani, H. Fukazawa, Y. Kohori, I. Watanabe, C. Sekine, and I. Shirotani, Phys. Rev. B **73**, 052408 (2006).

[8] S. H. Curnoe, H. Harima, K. Takegahara, and K. Ueda, Phys. B (Amsterdam, Neth.) **312–313**, 837 (2002).

[9] H. Sugawara, T. D. Matsuda, K. Abe, Y. Aoki, H. Sato, S. Nojiri, Y. Inada, R. Settai, and Y. Onuki, Phys. Rev. B **66**, 134411 (2002).

[10] K. Iwasa, Y. Watanabe, K. Kuwahara, M. Kohgi, H. Sugawara, T. D. Matsuda, Y. Aoki, and H. Sato, Phys. B (Amsterdam, Neth.) **312–313**, 834 (2002).

[11] M. Kohgi, K. Iwasa, M. Nakajima, N. Metoki, S. Araki, N. Bernhoeft, J M. Mignot, A. Gukasov, H. Sato, Y. Aoki, and H. Sugawara, J. Phys. Soc. Jpn. **72**, 1002 (2003).

[12] N. Takeda and Y. Ishikawa, J. Phys. Soc. Jpn. **69**, 868 (2000).

[13] K. Iwasa, S. Itobe, C. Yang, Y. Murakami, M. Kohgi, K. Kuwahara, H. Sugawara, H. Sato, N. Aso, T. Tayama, and T. Sakakibara, J. Phys. Soc. Jpn. **77**, 318 (2008).

[14] D. T. Adroja, J.-G. Park, K. A. McEwen, N. Takeda, M. Ishikawa, and J.-Y. So, Phys. Rev. B **68**, 094425 (2003).

[15] D. T. Adroja, J.-G. Park, E. A. Goremychkin, K. A. McEwen, N. Takeda, B. D. Rainford, K. S. Knight, J. W. Taylor, J. Park, H. C. Walker, R. Osborn, and P. S. Riseborough, Phys. Rev. B **75**, 014418 (2007).

[16] R. E. Baumbach, P. C. Ho, T. A. Sayles, M. B. Maple, R. Wawryk, T. Cichorek, A. Pietraszko, and Z. Henkie, Proc. Natl. Acad. Sci. USA **105**, 17307 (2008).

[17] S. Sanada, Y. Aoki, H. Aoki, A. Tsuchiya, D. Kikuchi, H. Sugawaray, and H. Sato, J. Phys. Soc. Jpn. **74**, 246 (2005).

[18] C. Sekine, T. Uchiumi, I. Shirotani, and T. Yagi, Phys. Rev. Lett. **79**, 3218 (1997).

[19] L. Bochenek, R. Wawryk, Z. Henkie, and T. Cichorek, Phys. Rev. B **86**, 060511(R) (2012).

[20] R. E. Baumbach, P. C. Ho, T. A. Sayles, M. B. Maple, R. Wawryk, T. Cichorek, A. Pietraszko, and Z. Henkie, J. Phys.: Condens. Matter **20**, 075110 (2008).

[21] T. A. Sayles, R. E. Baumbach, W. M. Yuhasz, M. B. Maple, L. Bochenek, R. Wawryk, T. Cichorek, A. Pietraszko, Z. Henkie, and P.-C. Ho, Phys. Rev. B **82**, 104513 (2010).

[22] A. Rudenko, Z. Henkie, and T. Cichorek, Solid State Commun. **242**, 21 (2016).

[23] G. Seyfarth, J. P. Brison, M.-A. Méasson, J. Flouquet, K. Izawa, Y. Matsuda, H. Sugawara, and H. Sato, Phys. Rev. Lett. **95**, 107004 (2005).

[24] W. Jeitschko and D. Braun, Acta Crystallogr., Sect. B: Struct. Sci. **33**, 3401 (1977).

[25] H. Sato, H. Sugawara, Y. Aoki, and H. Harima, in *Handbook of Magnetic Materials*, edited by K. H. J. Buschow (North-Holland, Amsterdam, 2009), Vol. 18, p. 1.

[26] C. Tarantini, A. Gurevich, J. Jaroszynski, F. Balakirev, E. Bellingeri, I. Pallecchi, C. Ferdeghini, B. Shen, H. H. Wen, and D. C. Larbalestier, Phys. Rev. B **84**, 184522 (2011).

[27] C. Ren, Z.-S. Wang, H.-Q. Luo, H. Yang, L. Shan, and H.-H. Wen, Phys. Rev. Lett. **101**, 257006 (2008).

[28] Y. Kasahara, T. Iwasawa, H. Shishido, T. Shibauchi, K. Behnia, Y. Haga, T. D. Matsuda, Y. Onuki, M. Sigrist, and Y. Matsuda, Phys. Rev. Lett. **99**, 116402 (2007).

[29] R. W. Hill, S. Li, M. B. Maple, and L. Taillefer, Phys. Rev. Lett. **101**, 237005 (2008).

[30] S. Kittaka, Y. Aoki, Y. Shimura, T. Sakakibara, S. Seiro, C. Geibel, F. Steglich, H. Ikeda, and K. Machida, Phys. Rev. Lett. **112**, 067002 (2014).

[31] Y. S. Hor, A. J. Williams, J. G. Checkelsky, P. Roushan, J. Seo, Q. Xu, H. W. Zandbergen, A. Yazdani, N. P. Ong, and R. J. Cava, Phys. Rev. Lett. **104**, 057001 (2010).

[32] J. L. Zhang, S. J. Zhang, H. M. Weng, W. Zhang, L. X. Yang, Q. Q. Liu, S. M. Feng, X. C. Wang, R. C. Yu, L. Z. Cao, L. Wang, W. G. Yang, H. Z. Liu, W. Y. Zhao, S. C. Zhang, X. Dai, Z. Fang, and C. Q. Jin, Proc. Natl. Acad. Sci. USA **108**, 24 (2011).

[33] T. Namiki, C. Sekine, K. Matsuhira, M. Wakeshima, and I. Shirotani, J. Phys. Soc. Jpn. **77**, 336 (2008).

[34] I. Shirotani, K. Ohno, C. Sekine, T. Yagi, T. Kawakami, T. Nakanishi, H. Takahashi, J. Tang, A. Matsushita, and T. Matsumoto, Physica B: Condens. Matter **281–282**, 1021 (2000).

[35] I. Shirotani, T. Uchiumi, K. Ohno, C. Sekine, Y. Nakazawa, K. Kanoda, S. Todo, and T. Yagi, Phys. Rev. B **56**, 7866 (1997).

[36] J. Klotz, K. Götze, V. Lorenz, Yu. Prots, H. Rosner, H. Harima, L. Bochenek, Z. Henkie, T. Cichorek, I. Sheikin, and J. Wosnitza, Phys. Rev. B **100**, 205106 (2019).

[37] M. M. Koza, D. A. Droja, N. T. Akeda, Z. Henkie, and T. Cichorek, J. Phys. Soc. Jpn. **82**, 114607 (2013).

[38] Y. Mizukami, M. Kończykowski, O. Tanaka, J. Juraszek, Z. Henkie, T. Cichorek, and T. Shibauchi, Phys. Rev. Res. **2**, 043428 (2020).

[39] Z. Henkie, M. B. Maple, A. Pietraszko, R. Wawryk, T. Cichorek, R. E. Baumbach, W. M. Yuhasz, and P.-C. Ho, J. Phys. Soc. Jpn. **77**, 128 (2008).

[40] J. E. Sonier, J. H. Brewer, and R. F. Kiefl, Rev. Mod. Phys. **72**, 769 (2000).

[41] F. L. Pratt, Phys. B (Amsterdam, Neth.) **289–290**, 710 (2000).

[42] A. Q. R. Baron, Y. Tanaka, S. Goto, K. Takeshita, T. Matsushita, and T. Ishikawa, J. Phys. Chem. Solids **61**, 461 (2000).

[43] G. Kresse and J. Furthmüller, Comput. Mater. Sci. **6**, 15 (1996).

[44] G. Kresse and D. Joubert, Phys. Rev. B **59**, 1758 (1999).

[45] J. P. Perdew, K. Burke, and M. Ernzerhof, Phys. Rev. Lett. **77**, 3865 (1996).

[46] H. J. Monkhorst and J. D. Pack, Phys. Rev. B **13**, 5188 (1976).

[47] K. Parlinski, in *Neutrons and Numerical Methods*, AIP Conf. Proc. No. 479 (AIP, Melville, NY, 1999), p. 121.

[48] J. Juraszek, R. Wawryk, Z. Henkie, M. Konczykowski, and T. Cichorek, Phys. Rev. Lett. **124**, 027001 (2020).

[49] B. D. Rainford and G. J. Daniell, Hyperfine Interact. **87**, 1129 (1994).

[50] A. Bhattacharyya, M. R. Lees, K Panda, P. P. Ferreira, T. T. Dorini, E. Gaudry, L. T. F. Eleno, V. K. Anand, J. Sannigrahi, P. K. Biswas, R. Tripathi, and D. T. Adroja, Phys. Rev. Mater. **6**, 064802 (2022).

[51] A. Bhattacharyya, D. T. Adroja, M. Smidman, and V. K. Anand, Sci. China Phys. Mech. Astron. **61**, 127402 (2018).

[52] A. Bhattacharyya, D. T. Adroja, K. Panda, S. Saha, T. Das, A. J. S. Machado, O. V. Cigarroa, T. W. Grant, Z. Fisk, A. D. Hillier, and P. Manfrinetti, Phys. Rev. Lett. **122**, 147001 (2019).

[53] K. Panda, A. Bhattacharyya, D. T. Adroja, N. Kase, P. K. Biswas, S. Saha, T. Das, M. R. Lees, and A. D. Hillier, Phys. Rev. B **99**, 174513 (2019).

[54] E. E. M. Chia, M. B. Salamon, H. Sugawara, and H. Sato, Phys. Rev. B **69**, 180509(R) (2004).

[55] R. Prozorov and R. W. Giannetta, Supercond. Sci. Technol. **19**, R41 (2006).

[56] J. F. Annett, Adv. Phys. **39**, 83 (1990).

[57] G. M. Pang, M. Smidman, W. B. Jiang, J. K. Bao, Z. F. Weng, Y. F. Wang, L. Jiao, J. L. Zhang, G. H. Cao, and H. Q. Yuan, Phys. Rev. B **91**, 220502(R) (2015).

[58] R. Khasanov, D. V. Evtushinsky, A. Amato, H.-H. Klauss, H. Luetkens, Ch. Niedermayer, B. Büchner, G. L. Sun, C. T. Lin, J. T. Park, D. S. Inosov, and V. Hinkov, Phys. Rev. Lett. **102**, 187005 (2009).

[59] S. Avci, O. Chmaissem, D. Y. Chung, S. Rosenkranz, E. A. Goremychkin, J. P. Castellan, I. S. Todorov, J. A. Schlueter, H. Claus, A. Daoud-Aladine, D. D. Khalyavin, M. G. Kanatzidis, and R. Osborn, Phys. Rev. B **85**, 184507 (2012).

[60] R. Khasanov and A. Shengelaya, *High-$T_c$ Superconductors and Related Transition Metal Oxides*, edited by A. Bussmann-Holder and H. Keller (Springer, Berlin, 2007), pp. 177–190.

[61] P. K. Biswas, A. Amato, C. Baines, R. Khasanov, H. Luetkens, H. Lei, C. Petrovic, and E. Morenzoni, Phys. Rev. B **88**, 224515 (2013).

[62] A. Bhattacharyya, K. Panda, D. T. Adroja, N. Kase, P. K. Biswas, S. Saha, T. Das, M. R. Lees, and A. D. Hillier, J. Phys.: Condens. Matter **32**, 085601 (2020).

[63] D. T. Adroja, A. Bhattacharyya, Y. J. Sato, M. R. Lees, P. K. Biswas, K. Panda, V. K. Anand, G. B. G. Stenning, A. D. Hillier, and D. Aoki, Phys. Rev. B **103**, 104514 (2021).

[64] A. Bhattacharyya, P. P. Ferreira, K. Panda, F. B. Santos, D. T. Adroja, K. Yokoyama, T. T. Dorini, L. T. F. Eleno, and A. J. S. Machado, J. Phys.: Condens. Matter **34**, 035602 (2022).

[65] A. Bhattacharyya, D. T. Adroja, J. S. Lord, L. Wang, Y. Shi, K. Panda, H. Luo, and A. M. Strydom, Phys. Rev. B **101**, 214437 (2020).

[66] See Supplemental Material at http://link.aps.org/supplemental/10.1103/PhysRevB.106.134516 for more information on the concise form of the inelastic x-ray data and their analysis.

[67] H. M. Tütüncü, E. Karaca, and G. P. Srivastava, Phys. Rev. B **95**, 214514 (2017).

[68] D. Adroja *et al.*, Muon spin rotation and relaxation studies of the multiband filled skutterudite superconductor $LaRu_4As_{12}$, STFC ISIS Neutron and Muon Source, (2016), doi: 10.5286/ISIS.E.79112107.